Computations of Turbulent Evaporating Sprays

S. K. Aggarwal* and S. Chitre†
University of Illinois at Chicago, Chicago, Illinois 60680

A computational study of turbulent evaporating sprays is reported. The major focus is to study the structure of turbulent evaporating sprays and to examine the sensitivity of their vaporization behavior to transient liquid-phase processes. Three models considered to represent these processes are the thin-skin, infinite-diffusion, and diffusion-limit models. Favre-averaged equations with a k-ε-g turbulence model are employed for the gas phase. The Lagrangian approach with a stochastic separated-flow method is used for the liquid phase where the effects of gas turbulence on droplet trajectories and interphase transport rates are considered using random-walk computations. Variable-property effects are also considered in a comprehensive manner. Results indicate that, depending upon the boiling temperature and heat of vaporization of the fuel considered, the vaporization behavior of turbulent sprays may be quite sensitive to the modeling of transient liquid-phase processes. Thus, it is important that for most hydrocarbon fuels these processes be adequately represented in comprehensive spray computations. The present results also provide further support to the conclusions of earlier studies which have been based on simplified spray configurations.

Nomenclature

a = acceleration of gravity
C_D = drag coefficient
c_p = gas specific heat
c_{pl} = liquid specific heat
d_p = droplet diameter
D = mass diffusivity
f = mixture fraction
g = square of mixture fraction fluctuation
h = heat transfer coefficient
k = turbulence kinetic energy
L = enthalpy of vaporization
Le = gas-phase Lewis number
$\dot{m}$ = drop mass
m'' = mass flux at drop surface
n_i = number of drops per unit time in group i
Pr = Prandtl number
r = radial distance in the jet
Re = Reynolds number
Sc = Schmidt number
S_ϕ = source term
$S_{p\phi}$ = droplet source term
t = time
T = gas temperature
T_b = boiling temperature
T_p = droplet surface temperature
T_l = liquid temperature
u = gas velocity (also axial gas velocity)
v = radial gas velocity
x = axial distance
α_l = liquid thermal diffusivity
Δt_p = time-step size for liquid-phase calculation
ε = rate of dissipation of turbulence kinetic energy
λ = thermal conductivity
μ_t = turbulent viscosity
ρ = gas density
ρ_p = liquid density
ϕ = generic variable

Subscripts

g = gas-phase property
i = droplet group
p = droplet property
∞ = ambient condition

Superscripts

$-$ = time (Reynolds) average
$\sim$ = Favre average

Introduction

THE development of comprehensive predictive capabilities for turbulent sprays depends on an accurate representation of the exchange processes between the gas and the liquid phases. Because the exchange rate terms are strongly sensitive to the droplet trajectory and vaporization rate, it is important that both be calculated accurately in any spray code. The droplet trajectory calculation largely depends upon the accuracy of the drag law employed and the modeling of drop-turbulence interactions. It is also affected by the vaporization rate prediction, because the latter determines the droplet size distribution in the spray. The accurate prediction of vaporization rate depends on 1) droplet surface temperature since the fuel vapor mass fraction at the surface generally has an exponential dependence on this temperature, 2) realistic representation of gas-phase convection, 3) variable-property effects because the thermophysical properties of the gas film outside the droplet can vary significantly during the droplet lifetime as it travels in a combusting environment, and 4) droplet trajectory calculations that determine the instantaneous droplet locations and hence the local environment for calculating the vaporization rate.

In the present paper, a computational study of turbulent evaporating sprays is reported. The major focus of the study is to advance the predictive capabilities for turbulent sprays and to present a detailed comparison of three vaporization models used to represent the transient heat transport within the droplet. The models considered are the thin-skin, infinite-diffusion, and diffusion-limit models. The sensitivity of the vaporization behavior of turbulent sprays to these models is examined. The present work is important because the current turbulent spray models[1,2] do not consider the transient processes within the droplet. Many recent studies[3-5] have indicated that the spray vaporization characteristics are strongly sensitive to the way the transient liquid-phase processes are modeled. These studies are, however, limited to idealized

Received May 16, 1989; revision received Dec. 6, 1989.

*Associate Professor, Department of Mechanical Engineering.
†Research Assistant, Department of Mechanical Engineering.

spray configurations; for example, one-dimensional laminar sprays. A comparison of various vaporization models in a more realistic turbulent spray is, therefore, of significant interest.

The present study is also important because the spray model developed here is quite comprehensive and provides an improvement over the existing models. In the previous studies, reviewed by Faeth,[2] either the liquid-phase transient processes are not considered, or the effect of gas-phase turbulence on the droplet dispersion and vaporization is not adequately represented. Also, the variable-property effects are generally not considered. In the present model, all of the above processes are represented in a more complete manner to study the detailed structure of turbulent evaporating sprays in a hot environment.

Physical Model

The physical model considers a pressure-atomized spray injected into a quiescent hot environment. An Eulerian-Lagrangian approach is employed to write the governing equations for the two phases. A parabolic flow configuration is assumed so that the boundary-layer approximations can be used for the continuous phase. The computation of the liquid phase is based on the solution of Lagrangian equations for each statistically significant sample or group of droplets. The stochastic separated flow (SSF) model[2] is employed to represent the effects of turbulent fluctuations on droplet trajectories, heating, and vaporization rates. The governing equations for both phases as well as the calculation procedure are essentially the same as those employed by Solomon et al.[1] The major difference from the cited reference is the representation of transient liquid-phase heat transport in the turbulent two-phase model, as discussed later.

Gas-Phase Equations

The equations for the continuous phase are based on the widely used k-ε-g turbulence model, because this approach has yielded good predictions for constant and variable density gas jets, particle-laden jets, and nonevaporating and evaporating sprays.[2,6,7] A steady axisymmetric low-Mach number turbulent jet flow with no swirl is considered. Major assumptions are that boundary-layer approximations are applicable, buoyancy only affects mean flow, exchange coefficients of all species and heat are equal, and kinetic energy is negligible. The Favre-averaged governing equations are employed, which can be written in a general form as

$$\frac{\partial}{\partial x}(\bar{\rho}\tilde{u}\tilde{\phi}) + \frac{1}{r}\frac{\partial}{\partial r}(r\bar{\rho}\tilde{v}\tilde{\phi}) = \frac{1}{r}\frac{\partial}{\partial r}\left(r\mu_{t\phi}\frac{\partial\tilde{\phi}}{\partial r}\right) + S_\phi + S_{p\phi} \tag{1}$$

where

$$\tilde{\phi} = \frac{\bar{\rho}\bar{\phi}}{\bar{\rho}} \tag{2}$$

is a Favre-averaged quantity and ϕ is a generic quantity. The conservation equations of mass, momentum, mixture fraction, turbulent kinetic energy, and rate of dissipation of turbulent kinetic energy obtained using Eq. (1) are given in Table 1. The expressions for $\mu_{t\phi}$, S_ϕ, and $S_{p\phi}$ along with the appropriate empirical constants are also given in the table. The mass and momentum source terms $S_{p\phi}$ appearing in gas-phase equations are obtained by computing the net change of mass and momentum of each droplet group i passing through a computational cell j. These can be written as

$$S_{pmj} = V_j^{-1}[\Sigma n_i(m_{i_{\text{in}}} - m_{i_{\text{out}}})]_j \tag{3a}$$

$$S_{puj} = V_j^{-1}[\Sigma n_i(m_i u_{pi})_{\text{in}} - (m_i u_{pi})]_{\text{out}} + m_i a[(1-\rho/\rho_p)\,\Delta t_p]_j \tag{3b}$$

Table 1 Source terms in Eq. (1)

ϕ	S_ϕ	$S_{p\phi}$
1	0	S_{pm}
u	$a(\rho_\infty - \bar{\rho})$	S_{pu}
f	0	S_{pm}
k	$\mu_t\left(\frac{\partial u}{\partial r}\right)^2 - \bar{\rho}\varepsilon$	0
ε	$(C_{\varepsilon 1}\mu_t\left(\frac{\partial u}{\partial r}\right)^2 - C_{\varepsilon 2}\bar{\rho}\varepsilon)(\varepsilon/k)$	0
g	$C_{g1}\mu_t\left(\frac{\partial f}{\partial r}\right)^2 - C_{g2}\bar{\rho}g\varepsilon/k$	0

C_μ	$C_{\varepsilon 1}$	C_{g1}	$C_{\varepsilon 2} = C_{g2}$	σ_k	σ_ε	$\sigma_f = \sigma_g$	Sc
0.09	1.44	2.9	1.87	1.0	1.3	0.7	0.7

Here n_i is the number of droplets in group i, m_i the mass of each droplet, and V_j the volume of computational cell j. Note that there are no droplet source terms in the equations for k, ε, and g due to the dilute spray approximation. The turbulent viscosity is calculated from

$$\mu_t = C_\mu \bar{\rho} k^2/\varepsilon \tag{4}$$

The Favre-averaged value of any scalar property is obtained from the state relationships $\phi(f)$ as follows

$$\tilde{\phi} = \int_0^1 \phi(f)\tilde{P}(f)\,\mathrm{d}f \tag{5}$$

while ρ is obtained from

$$\bar{\rho}^{-1} = \int_0^1 \frac{1}{\rho(f)}\tilde{P}(f)\,\mathrm{d}f \tag{6}$$

Following Solomon et al.,[1] the probability density function $\tilde{P}(f)$ is assumed to be a clipped Gaussian. The most probable value μ and standard deviation σ are determined from the calculated values of $\tilde{f}$ and g by using a table-look-up procedure. The state relationships are found by assuming adiabatic mixing of fuel and air, the latter being at a high temperature. The calculation of the thermodynamic equilibrium state then provides $\phi(f)$, where ϕ is any scalar property such as temperature, density, and mass fractions.

The numerical solution of the gas-phase equations is obtained by using a modified version of GENMIX.[1] Further details of the numerical algorithm can be found in the cited reference.

Liquid-Phase Equations

The Lagrangian approach in conjunction with the SSF method is employed to compute the properties of each group of droplets as it travels in the hot turbulent jet flow. The procedure is adopted from the work of Solomon et al.[1] The major assumptions in writing the Lagrangian equations are no direct droplet-droplet interaction, quasisteady gas phase, negligible radiation effects, drag law and the effects of forced convection as given by semiempirical relations,[2] and phase equilibrium at the drop surface. The equations governing the variation of position, velocity, and size for each droplet group i along its trajectory are

$$\frac{\mathrm{d}x_{pi}}{\mathrm{d}t} = u_{pi} \tag{7}$$

$$m_i\frac{\mathrm{d}u_{pi}}{\mathrm{d}t} = -\frac{\pi}{8}\mathrm{d}_{pi}^2\rho C_D|u_{pi}-u|(u_{pi}-u) + a \tag{8}$$

$$\frac{d\,\mathrm{d}_{pi}}{\mathrm{d}t} = -2\dot{m}_i''/\rho_p \tag{9}$$

where

$$\frac{\dot{m}_i''\,\mathrm{d}_{pi}}{\rho D} = 2N_s\ell n(1+B) \tag{10}$$

$$B = (Y_{FS} - Y_{F\infty})/(1 - Y_{FS}) \tag{11}$$

$$C_D = 24/Re[1 + (Re^{2/3}/6), \quad Re < 1000 \tag{12a}$$

$$C_D = 0.44, \quad Re > 1000 \tag{12b}$$

$$Re = \mathrm{d}_{pi}|u_{pi} - u|/v \tag{13}$$

Note that x_p, u_p, u, and a are vector quantities. The mass fraction of fuel vapor at the drop surface is obtained by using a phase equilibrium relation. The expression for N_s is given in the Appendix.

As noted earlier, an SSF model is employed to represent the effects of gas-phase turbulence on droplet trajectories as well as on droplet heating and vaporization rates. A Monte Carlo method is used to compute the trajectory of each droplet sample as it encounters a random distribution of turbulent eddies. There are two steps involved in this computation. In the first step, the instantaneous properties of each eddy, which includes the instantaneous velocity components and the scalar properties, are obtained. The velocity components are found by making a random selection from the probability density function of velocity, which is assumed to be Gaussian having a standard deviation of $(2k/3)^{1/2}$ and mean components $\tilde{u}$, $\tilde{v}$, 0. The instantaneous scalar properties are obtained in a similar manner. At any given physical location, the clipped Gaussian probability density function (PDF) of Y_F is constructed from the values of μ and σ, which are obtained from the known values of $\tilde{Y}_F$ and g. This Favre PDF is used to obtain a time-averaged PDF $\bar{P}(Y_F)$, which is then used to construct the cumulative PDF for f. This cumulative PDF is randomly sampled by selecting a random number between 0 and 1 to find the instantaneous value of f, which is then used in the state relationships to find the instantaneous temperature, composition, and density of the eddy. The second step involves specifying the time of interaction of a drop with the eddy, which is taken to be the smaller of the eddy lifetime and the drop transit time through the eddy.

The number of random walks for each droplet group varies from 3 to 9 in the present calculations. The random properties of each eddy, as calculated above, are used to advance the Lagrangian solution of Eqs. (7–9) for the position, velocity, and size of each droplet group. In these equations, the droplet surface temperature is an unknown and may have a strong effect on the accuracy of drop calculations, because the mass fraction of fuel vapor at the drop surface has an exponential dependence on this temperature. The three vaporization models examined in the present study differ essentially in the calculation of this temperature, as described in the following.

Thin-Skin Model

Here the transient heat transport within the droplet is completely neglected. It is assumed that the droplet surface adapts instantaneously to the changes in ambient conditions. To facilitate the computations, a table is constructed which gives the surface temperatures for selected values of f and Re. The procedure to construct the table is given in the Appendix.

For a given droplet sample, knowing its location, the instantaneous values of f and Re are calculated at that location. A table-look-up procedure then yields the droplet surface temperature. Thus the droplet temperature along its trajectory can be easily calculated.

Infinite-Diffusion Model

It is more appropriate to call this an infinite-conduction model when a single-component liquid fuel is considered. This model is basically the same as the thin-skin model except that the liquid thermal inertia is considered. It is assumed that the temperature is uniform inside the droplet but varies temporally. Using the energy balance for the droplet, the temporal variation of liquid temperature can be written as

$$\frac{\mathrm{d}T_p}{\mathrm{d}t} = \frac{6\dot{m}''(H-L)}{c_{pl}\rho_p\,\mathrm{d}_p} \tag{14}$$

where H is the amount of heat transferred to the droplet per unit liquid mass vaporized and is given by

$$\dot{m}''H = h(T - T_p) \tag{15}$$

and h is given in the Appendix. Note that H includes the heat of vaporization and that used for droplet heating.

Diffusion-Limit Model

In this model, the liquid temperature varies temporally as well as spatially. The transient heat transport within the droplet is represented by the unsteady heat diffusion equation in a spherically symmetric geometry. The solution of this equation involves a moving boundary-value problem as the droplet is evaporating. This problem can be avoided by using a transformation to make the boundary stationary. The transformed governing equation is

$$\frac{\partial \bar{T}_l}{\partial t} = \frac{1}{\bar{r}^2}\frac{\partial}{\partial \bar{r}^2}\left(\bar{r}^2\frac{\partial \bar{T}_l}{\partial \bar{r}}\right) - \frac{\bar{r}\bar{m}\lambda}{C_p Le\rho_p\alpha_l}\left(\frac{\partial \bar{T}_l}{\partial \bar{r}}\right) \tag{16}$$

with the boundary conditions as

$$\frac{\partial \bar{T}_l}{\partial \bar{r}} = 0 \quad \text{at} \quad \bar{r} = 0 \tag{17}$$

$$\frac{\partial \bar{T}_l}{\partial \bar{r}} = \frac{\bar{m}(H-L)\lambda}{c_p Le\lambda_l(T_B - T_0)} \quad \text{at} \quad \bar{r} = 1 \tag{18}$$

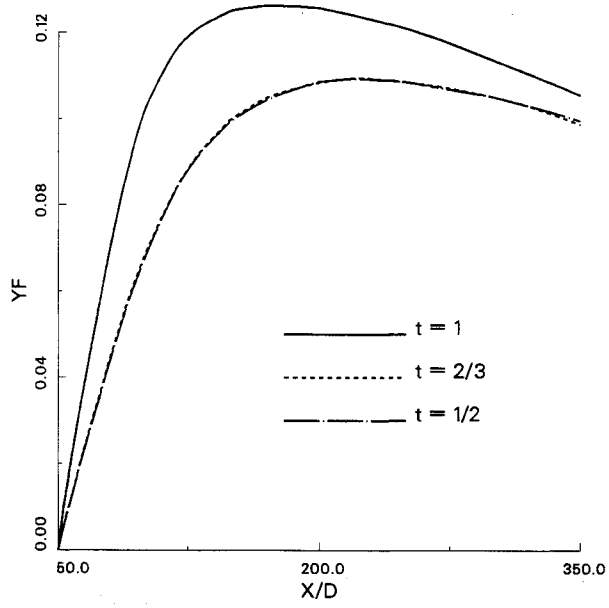

Fig. 1 Fuel vapor mass fraction along the jet axis for the diffusion-limit model; shows the step size independence ($t = 1$ corresponds to a time step size $= 1/20$ of the droplet transient time between two adjacent axial stations).

where $\bar{T}_l(\bar{r},\bar{t})$ and $\bar{r}$ are, respectively, the normalized liquid temperature and radial location inside the droplet, and $\bar{t}$ is the normalized time variable. These are given by

$$\bar{T}_l = (T_l - T_0)/(T_b - T_0) \tag{19a}$$

$$\bar{r} = 2r/d_p \tag{19b}$$

$$\bar{t} = \alpha_l \int_0^t \frac{4}{d_p^2}\, dt \tag{19c}$$

A second-order Crank-Nicolson implicit scheme with a variable grid size is employed to solve Eq. (16). Thus, the diffusion-limit model involves the solution of a partial differential equation for each statistically significant group of droplets. The instantaneous gas-phase properties required in this solution are again obtained by using the SSF methodology.

Results

The influence of liquid-phase models on the turbulent spray behavior is investigated by comparing the structures of evaporating sprays as predicted by the three models. To assess the effects of fuel properties, computations are reported for an *n*-heptane spray and a methanol spray injected into a hot quiescent environment, which is at a temperature of 800 K. Note that only those aspects that pertain to the effects of vaporization models are highlighted here. For example, gas-phase and droplet velocities are not discussed and can be found in Ref. 1. The initial conditions for the computations are taken from the experimental data of Solomon et al.,[1] at an axial location of $x/D = 50$. Note that the experimental data are for a Freon-11 spray with a Sauter mean diameter (SMD) of 60 μ. Although the data are not for the same fuel, they are still preferable to specifying some ad hoc initial conditions. Moreover, these experiments provide almost a complete set of initial conditions that include the radial profiles of mean and fluctuating velocities and of turbulent kinetic energy for the gas phase. The initial liquid-phase properties include radial profiles of liquid flux, drop-size distribution, and mean and fluctuating drop velocity at $x/D = 50$. The drop-size distribution consists of ten sizes ranging from 15 to 110 μ. In order to provide sufficient resolution of the liquid-phase properties, 200 droplet groups are used. In conjunction with ten sizes and three random walks employed in the SSF model, it amounts to a total of 6000 droplet groups that are tracked in the Lagrangian calculations. In order to assess the effects of the number of walks, some of the computations have also used 18,000 droplet samples.

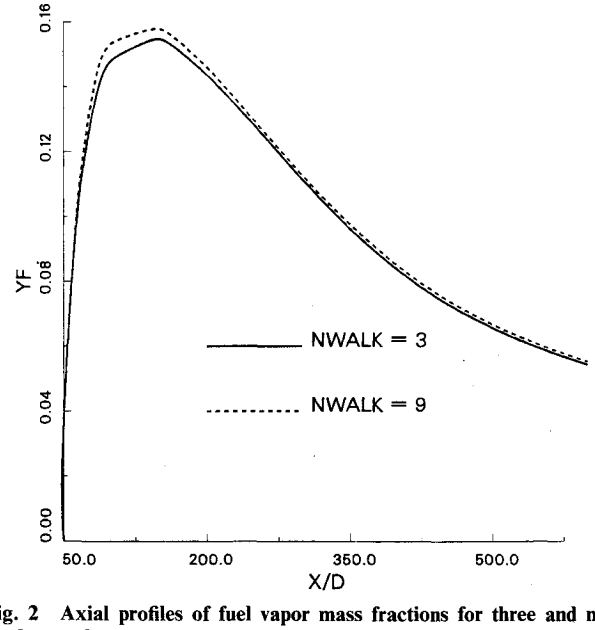

Fig. 2 Axial profiles of fuel vapor mass fractions for three and nine random walks.

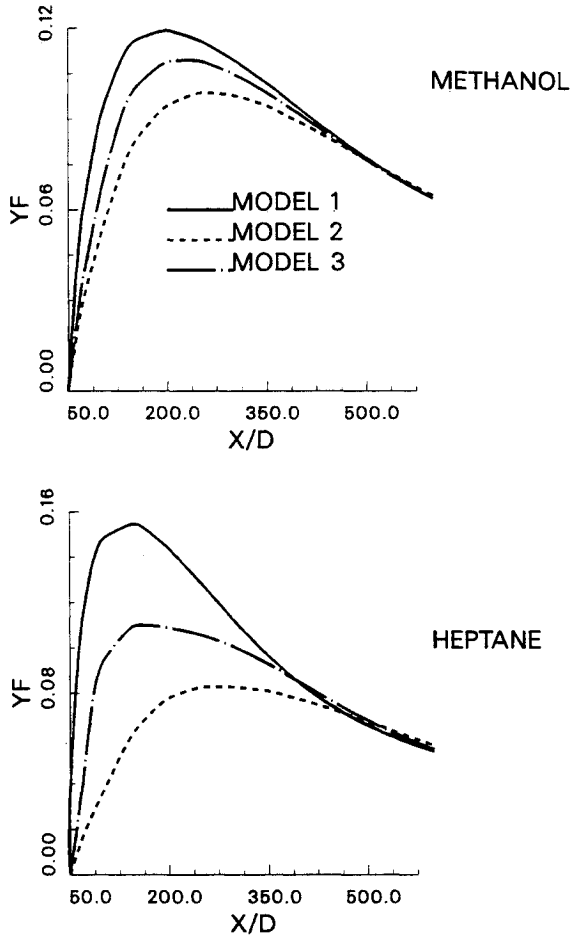

Fig. 3 Variation of fuel vapor mass fraction along the jet axis for heptane and methanol fuels; model 1—thin skin, model 2—infinite diffusion, model 3—diffusion limit.

The first set of results is aimed at assessing the step-size independence of the results. Figure 1 shows the variation of fuel vapor mass fraction along the jet axis for three values of the temporal step size used for integrating the liquid-phase equations. The diffusion-limit model is employed for these computations. Note that $t = 1$ corresponds to a temporal step size of 1/20th of the droplet transit time between two adjacent axial locations x and $x + dx$. As indicated in the figure, the fuel vapor mass fraction increases along the axis, reaches a peak value, and then decreases. The important observation is that for $t = 203$, the predictions are almost independent of the temporal step size. Thus all computations reported here are based on this temporal step size. It should also be noted that the spatial step sizes for discretizing the gas-phase equations are automatically controlled in the computations, and the effects of these sizes have been examined in the earlier studies.[1,2]

Another important parameter in the computations is the number of random walks used for the SSF model. Its effect on the numerical results is illustrated in Fig. 2, where the fuel vapor distributions in the axial direction are compared for three and nine random walks. These results are obtained by using the thin-skin model; the behavior is similar with the other two models. As indicated, increasing the number of walks from 3 to 9 causes only a small quantitative change in predictions. The overall conclusion is that with three random walks, the SSF model yields results which are reasonably independent of the number of walks.

Figure 3 shows the variation of fuel vapor mass fraction along the jet axis predicted by the three models. The corre-

sponding radial profiles at three axial locations are given in Fig. 4. Results are shown for both n-heptane and methanol sprays. Note that the fuel vapor mass fraction is assumed to be zero at the initial station $x/D = 50$. In all the figures, models 1, 2, and 3 refer to thin-skin, infinite-diffusion, and diffusion-limit models, respectively. The important observations are as follows:

1) The general qualitative behavior for all three models is similar. As the result of vaporization, the fuel vapor mass fraction increases along the spray axis for all three models until the fraction reaches a maximum value at some location. Further downstream, the effect of turbulent mass diffusion in the radial direction becomes more dominant compared to that of vaporization, and consequently the fuel vapor mass fraction then decreases slowly. This behavior is observed for both fuels except that the maximum value of vapor mass fraction is attained earlier for heptane (at about $x/D = 125$) than for methanol where the peak occurs at about $x/D = 200$. This indicates that the vaporization rate is somewhat higher for heptane than that for methanol. This is the result of the heat of vaporization of methanol being about 3.5 times greater than that of heptane.

2) As seen in Fig. 4, the fuel vapor mass fraction generally has its maximum value at or near the spray axis because the liquid mass flux initially is the maximum there, although the gas temperature is the lowest in the jet interior.

3) Perhaps the most important observation here is the difference in the degree of sensitivity exhibited by the two sprays to the liquid-phase models. The vaporization behavior of heptane spray displays strong sensitivity to the models used. The methanol spray behavior, however, does not seem to be affected much by the models. This is reflected both in the axial and radial distributions of fuel vapor mass fraction. The divergence in sensitivity can be attributed to the differences in the vaporizing characteristics of the two fuels, i.e., their boiling temperature and heat of vaporization. The boiling temperature of heptane is 372 K, which is relatively high compared to a value of 338 K for methanol. Because the initial liquid temperature is assumed to be 300 K, there is less droplet heating involved for methanol droplets compared to heptane droplets. Consequently, the effect of different liquid-phase models is not as significant for the methanol case, because the models differ essentially in the prediction of droplet surface temperature. In addition, the heat of vaporization of methanol is about 3.5 times higher than that of heptane, which further reduces the role of droplet heating in the vaporization process for methanol.

4) The thin-skin model consistently overpredicts the fuel vapor mass fraction as compared to the infinite-diffusion and diffusion-limit models. This is because the liquid thermal inertia is completely neglected in this model, because the droplet surface temperature is assumed to adjust instantaneously to the local environment. Consequently, the model overpredicts the surface temperature that results in the overprediction of the fuel vapor mass fraction at the drop surface, which has an exponential dependence on temperature. As a result, the vaporization rate is overestimated by the model. This is further demonstrated in Fig. 5, where the droplet diameter history, predicted by the three models, is compared. As noted earlier, these computations employ 6000 droplet samples consisting of 200 initial locations, 10 size groups, and 3 random walks. Figure 5 shows the variation of instantaneous diameter for a droplet sample, which is initially at the jet axis and belongs to the size group number 6 (initial diameter of 65 μ). Also note that the fluctuations in the instantaneous droplet diameter are because the droplets transverse a turbulent flowfield where the gas-phase properties are changing spatially as well as temporally; the latter is the result of turbulent fluctuations. It is further worth mentioning that the mean gas temperature is decreasing along the droplet

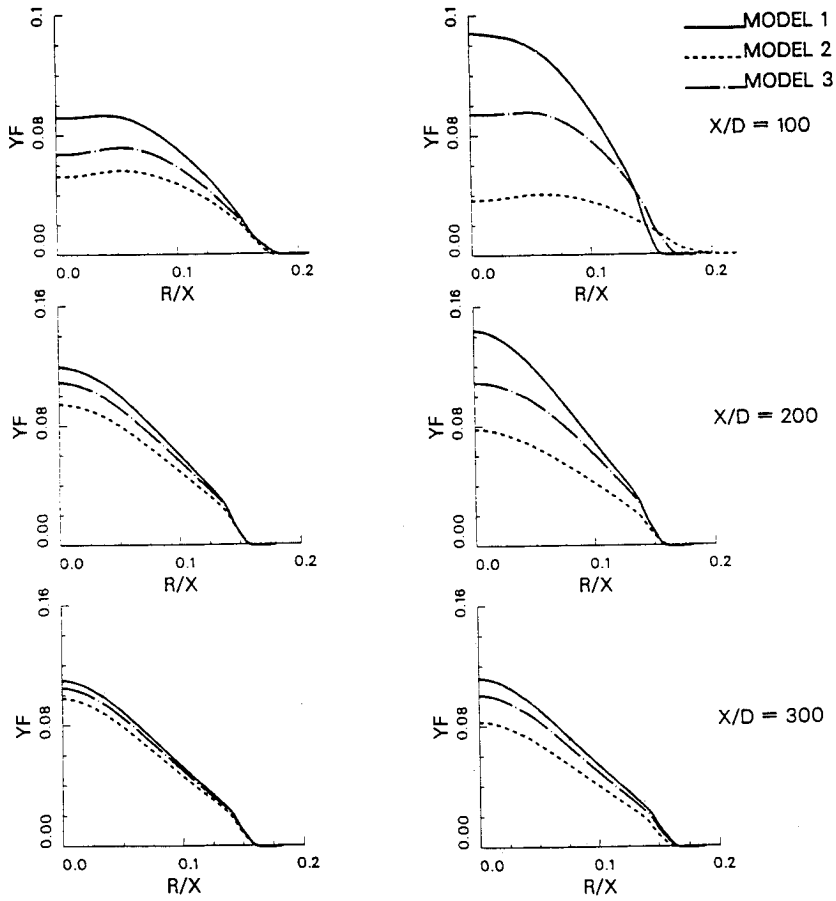

Fig. 4 Radial variation of fuel vapor mass fraction for heptane and methanol fuels.

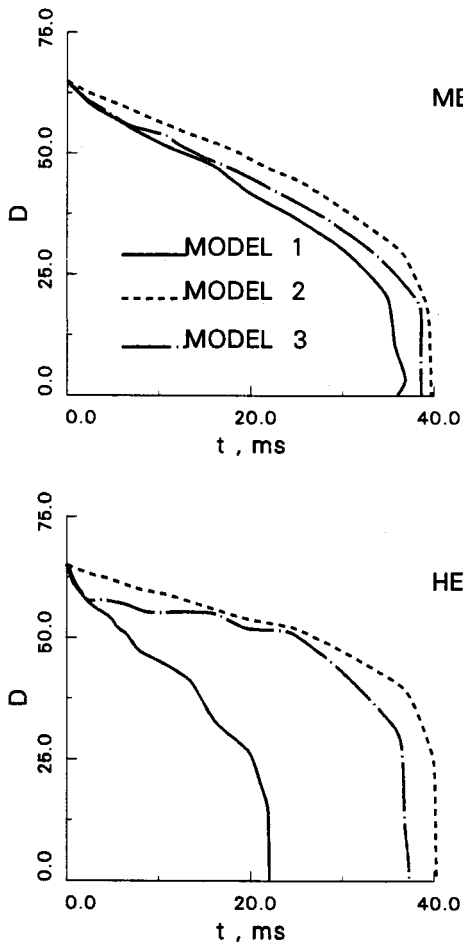

Fig. 5 Variation of droplet diameter (droplet group number 6) with time as predicted by thin-skin, infinite-diffusion, and diffusion-limit models; initial diameter is 65 μ.

trajectory, and as a result, the rate of change of droplet diameter decreases with time. However, the droplet diameter is getting smaller, which increases the rate of change of diameter with time because the rate varies inversely with diameter. As clearly indicated in Fig. 5, the thin-skin model overpredicts the vaporization rate compared to the other two models. This results in the higher value of fuel vapor mass fraction in the jet, as shown in Figs. 3 and 4. The degree of overprediction depends upon the vaporization characteristics of fuel. For example, the differences between the thin-skin and other two models are much more significant for heptane than for methanol. This is clearly demonstrated by the droplet diameter history plots in Fig. 5 as well as by the variation of fuel vapor mass fraction in Figs. 3 and 4, as discussed earlier. For heptane, the droplet lifetime predicted by the thin-skin model is only about one-half of that predicted by the other two models. For methanol, however, the predictions by the three models are nearly the same. Correspondingly, the values of fuel vapor mass fraction predicted by the thin-skin and infinite-diffusion models differ as much as 100% for heptane but only about 20% for methanol. The results in Fig. 4 exhibit a similar behavior.

5) The comparison of models 2 and 3 indicates that the diffusion-limit model generally gives a higher fuel vapor mass fraction than the infinite-diffusion model, because the heat is transferred from the gas-phase remains near the surface region and is not conducted to the droplet interior for the diffusion-limit model. On the other hand, the heat is distributed uniformly inside the droplet for the infinite-diffusion case. As a result, model 3 initially predicts a higher surface temperature and, therefore, higher vaporization rate compared to model 2. This is clearly shown by the drop diameter history plots in Fig. 5 and the fuel vapor mass fraction profiles in Figs. 3 and 4. The trend reverses, however, during the latter part of the droplet lifetime as reflected in the fuel vapor mass fraction profiles in Fig. 3. Thus, the conclusions of earlier studies,[3,4] which employed idealized configurations, are supported in a more realistic spray situation here.

The variation of SMD along the jet axis is shown in Fig. 6. Again the results are given for methanol and heptane sprays. For most of the jet, the axial distribution of SMD is qualitatively similar for the three models. The SMD first decreases (for x/D between 50 and 150) as the droplets are vaporizing and then increases with x/D before it drops to zero. The increase of SMD in the axial direction is quite typical for polydisperse sprays. It is caused by the complete vaporization of smaller droplets, which effectively increases the SMD. Also, the vaporization process is essentially completed at $x/D = 400$ for all three models, although it is not quite apparent in the SMD plots. This is more of a statistical aberration because SMD represents an average drop size for the remaining droplets; note that the maximum drop size considered is 105 μ. The important observation from Fig. 6 is that the quantitative differences in the SMD distributions predicted by the three models are quite substantial for heptane but relatively insignificant for methanol. Similar differences are observed, though not shown here, in the radial profiles of SMD. These results are consistent with those shown in Figs. 3 and 4.

The comparison of droplet trajectories in the jet for the three models is illustrated in Fig. 7, where the position of a 65 μ (initial diameter) droplet group is plotted. It is clearly indicated that the trajectory computation is also sensitive to the droplet vaporization models, because the models influence the droplet size calculation, as indicated in Figs. 5 and 6, as

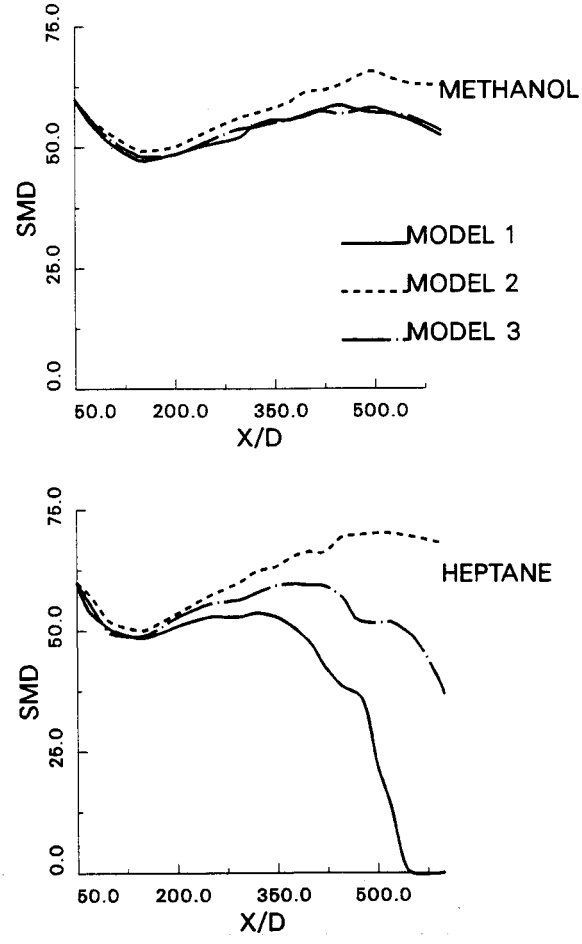

Fig. 6 SMD variation along the jet axis as predicted by three models.

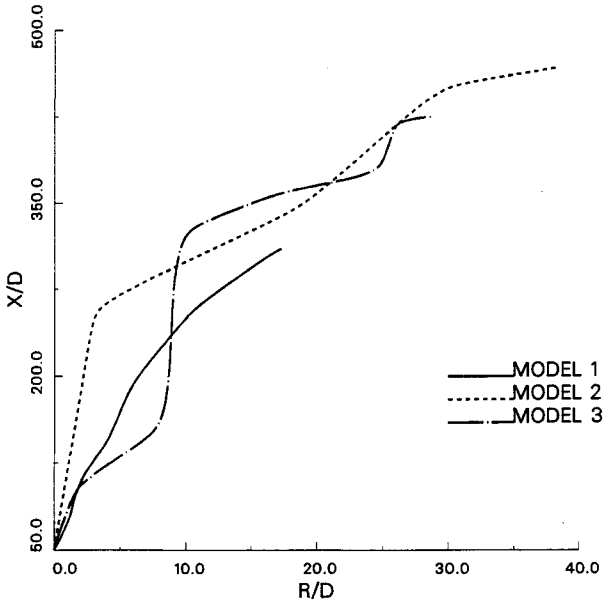

Fig. 7 Trajectory of the 65 μ (initial diameter) droplet group in the jet for the three models (heptane spray).

well as the gas phase properties, as indicated in Figs. 3 and 4. The present study thus provides a clear indication that the transient liquid-phase processes are important and should be adequately represented in more comprehensive spray computations.

Another important aspect regarding the comparison of models is the increase in the computational effort due to the implementation of advanced liquid-phase models in comprehensive turbulent spray calculations. The comparison of CPU times for the models indicates that the increase in the CPU time is large but not prohibitively so. The CPU times on a Cray-XMP machine for calculating the heptane spray for x/D of 600 and with 6000 droplet samples were 650, 6305, and 5781 s for models 1, 2, and 3 respectively. Note that more CPU time is indicated for the infinite-diffusion model compared to the diffusion-limit model, which is somewhat misleading. This is because the time-step size for droplet calculation is controlled automatically depending upon the droplet size. It is also noteworthy that the increase in CPU time for models 2 and 3 is, to a large extent, due to the comprehensive calculations of variable thermophysical properties along the trajectory of each droplet group; this calculation is avoided with model 1 where a table-look-up procedure is used. In addition, as a result of the parabolic flow situation considered here, the CPU time for the gas-phase computation is negligibly small compared to the liquid-phase computation. Perhaps, the comparison will look more favorable for the computation of sprays in recirculating flow situations.

Conclusions

A comprehensive model is developed for predicting the detailed structure of turbulent sprays. The important features of the model are that a k-ε-g turbulent model is used for the Favre-averaged gas-phase equations, an SSF random-walk method is employed to account for the effects of gas-phase turbulence on droplet trajectory and vaporization, the variable-property effects are considered in detail, and the transient liquid-phase processes are adequately represented. The predictions are shown to be reasonably independent of the step sizes.

The detailed structures of two turbulent evaporating sprays are reported, and their sensitivity to the vaporization models is studied. The models considered are the thin-skin, infinite-diffusion, and diffusion-limit models. The computations are started at an axial station of $x/D = 50$, where the experimental data of Solomon et al.,[1] have been used for initial conditions. The major conclusions is that the vaporization behavior of turbulent sprays is strongly sensitive to the vaporization models used to represent the transient heat transport within the droplets. Although the degree of sensitivity is dependent upon the boiling temperature and the heat of vaporization of fuel considered, a strong sensitivity can be expected for most hydrocarbon fuels. The present study is also useful in the sense that the conclusions of earlier studies[3-4] that employed simplified spray configurations are now validated for more realistic turbulent sprays.

As a concluding remark, it is hoped that the computational results presented here would motivate experimentalists to provide similar or other bench-mark type measurements for turbulent evaporating sprays. In this regard, it should be mentioned that further improvements in the vaporization models can be easily implemented in the comprehensive spray model generated in the present study. For example, the improved C_D correlations to incorporate the mass transfer effects and the effective diffusivity model to include the effect of liquid circulation within the droplets[8] can be easily included.

Appendix: Procedure to Construct a Table for T_p, f, Re

1) Select the values of f and Re.

2) Find the ambient properties such as temperature, density, and mass fractions corresponding to the f value by using the state relationships.

3) Assume a value for T_p and calculate the fuel vapor mass fraction at the drop surface from the phase equilibrium equation.

4) Calculate the average mixture properties in the gas layer outside the droplet by using a suitable weighted average of surface and ambient values, i.e.,

$$\phi_{\text{ave}} = \alpha\phi_{gs} + (1-\alpha)\phi_{g\infty}$$

where α is assumed to be 0.7 in the present study.

5) Using the average values, calculate the thermophysical properties such as μ, k, D, c_p, Le, Pr, and Sc.

6) Use the following equation to get a new value of T_p

$$h(T - T_p)\dot{m}''L$$

where

$$\frac{h\,\mathrm{d}_p}{k} = \frac{2(N_p/Le)\,\ell n(1+B)}{(1+B)^{1/Le}-1}$$

$$\frac{\dot{m}''\,\mathrm{d}_p}{\rho D} = 2N_s\,\ell n(1+B)$$

$$N_p \text{ or } N_s = \frac{1+0.276Re^{1/2}(Pr \text{ or } Sc)^{1/3}}{1+1.232/[Re(Pr \text{ or } Sc)^{4/3}]}$$

$$B = (Y_{FS} - Y_{F\infty})/(1 - Y_{FS})$$

7) Repeat steps 3–6 until the required convergence is achieved.

8) Repeat the procedure for other values of f and Re.

Note that the droplet size does not change during this calculation for the thin-skin model.

Acknowledgment

This work has been supported by a grant from the NASA Lewis Research Center under the technical direction of D. Bulzan, Institute of Computational Mechanics in Propulsion (ICOMP), and a National Science Foundation grant for the use of the Supercomputer Cray-XMP. Many fruitful discussions with J. S. Shuen at NASA Lewis Research Center are also appreciated.

References

[1]Solomon, A. S. P., Shuen, J. S., Zhang, Q. F., and Faeth, G. M., "Measurements and Predictions of the Structures of Evaporating Sprays," *Journal of Heat Transfer*, Vol. 107, Aug. 1985, pp. 679–686.

[2]Faeth, G. M., "Evaporation and Combustion of Sprays," *Progress in Energy and Combustion Science*, Vol. 9, 1983, pp. 1–76.

[3]Aggarwal, S. K., Tong, A., and Sirignano, W. A., "A Comparison of Vaporization Models for Spray Calculations," *AIAA Journal*, Vol. 22, No. 10, 1984, pp. 1448–1457.

[4]Sirignano, W. A., "Fuel Vaporization and Spray Combustion Theory," *Progress in Energy and Combustion Science*, Vol. 9, 1983, pp. 291–322.

[5]Aggarwal, S. K., "Modeling of Multicomponent Fuel Spray Vaporization," *International Journal of Heat Mass Transfer*, Vol. 30, No. 9, 1987, pp. 1949–1961.

[6]Solomon, A. S. P., Shuen, J. S., Zhang, Q. F., and Faeth, G. M., "Structure of Nonevaporating Sprays, Part I: Initial Conditions and Mean Properties," *AIAA Journal*, Vol. 23, No. 10, 1985, pp. 1548–1555.

[7]Solomon, A. S. P., Shuen, J. S., Zhang, Q. F., and Faeth, G. M., "Structure of Nonevaporating Sprays, Part II: Drop and Turbulence Properties," *AIAA Journal*, Vol. 23, No. 11, 1985, pp. 1724–1730.

[8]Sirignano, W. A., private communications, 1988.